IEEE Access
Multidisciplinary | Rapid Review | Open Access Journal

Received 10 October 2022, accepted 24 October 2022, date of publication 3 November 2022, date of current version 8 March 2023.

*Digital Object Identifier 10.1109/ACCESS.2022.3219130*

RESEARCH ARTICLE

# Direct Thrust Force Fault-Tolerant Control of Primary Permanent Magnet Linear Motor With Single DC-Link Current Sensor for Metro Application

**QIANGGUO YU[1], YANAN FENG[1], XU HUANG[1], PEILIANG WANG[2], AND MENGJIA ZENG[1]**
[1]School of Science and Engineering, Huzhou College, Huzhou, Zhejiang 313000, China
[2]School of Engineering, Huzhou University, Huzhou, Zhejiang 313000, China

Corresponding author: Yanan Feng (fengyanan@zjhzu.edu.cn)

This work was supported by the National Natural Science Foundation of China under Project 61573137.

**ABSTRACT** In order to improve the fault-tolerant control (FTC) ability of the current sensor of the primary permanent magnet linear motor (PPMLM) drive system, the direct thrust force control (DTFC) strategy with single DC-link current sensor is proposed. According to the principle of voltage vector equivalence, the present basic voltage vector is equivalent to two adjacent sub-basic voltage vectors to achieve the equivalence of the present candidate voltage vector. The principle of different phases based on the fact that the DC-link current is equal to or opposite to one of the phase currents is introduced. The output sequence of the two sub-basic voltage vectors is determined by the principle of different phase mode to ensure that the measured currents in the two adjacent periods are any two-phase currents in the three phases, and then the third-phase current is calculated. Finally, the effectiveness and correctness of the proposed DTFC (P-DTFC) is verified by simulation and experiment.

**INDEX TERMS** Primary permanent magnet linear motor (PPMLM), fault-tolerant control (FTC), equivalent voltage vector, direct thrust force control (DTFC), current sensor.

## I. INTRODUCTION

In recent years, the urban rail transit drive system has been favored by the governments on account of its fast and convenience. Compared with rotary motor drive systems, linear motor drive systems have many advantages [1], [2], [3], [4]. As a result of high power density, small size and light weight, permanent magnet linear motors (PMLMs) are get more and more concerns [5], [6], [7]. Meanwhile, PMLMs with unique merits are widely used in various industries [8], [9]. However, in urban rail transit long-distance transportation systems, the high engineering cost and difficult maintenance in the later period must be lead into, whether the permanent magnets (PM) or armature windings is laid on the track. In view of it, the primary PMLM (PPMLM) is proposed, in which the permanent magnets and armature windings are all mounted on the mover, while the stator is only composed of silicon steel sheets [10], [11], [12].

At present, because of fast dynamic response and high robustness, direct thrust force control (DTFC) has been widely used in linear motor traction systems [13], [14], [15]. Furthermore, in voltage-integral DTFC strategy, only the parameter resistance of motor which can be seen as the constant because of minimal change in spite of the motor is running compared with inductance is needed. In long-distance transportation systems, the linear encoder which is mounted on the track and exposed to harsh environments to get the electrical angle are bound to fail when the PMLM is adopted. So the voltage-integral DTFC strategy not only has higher robustness while the parameter of motor is changing, but also has better fault tolerance when the linear encoder fails [16], [17], [18].

The associate editor coordinating the review of this manuscript and approving it for publication was Christopher H. T. Lee.

Generally, three current sensor, a DC-link current sensor and two phase current sensor, are needed in a single PPMLM drive system. Meanwhile, the urban rail transit traction system is a multi-motor traction system, in which a large of current sensor are applied and the failure rate of current sensors must be increased inevitably [11], [19], [20]. Meanwhile, the accurate value of phase currents are demanded in motor drive, and the control performances will be seriously affected by current sensor faults [21], [22], [23]. Therefore, Current sensor FTC (CSFTC) is very important for urban rail transit systems, which has been paid widespread attentions and gets a rapid development in the academic community [24], [25], [26]. So for, a lot of PWM-based control methods using single DC-link current sensor which cannot be used for the look-up-table-based DTFC have been proposed [27], [28], [29]. In the PWM-based control methods, the reconstruction precision is largely affected by the dead zones, and the additional efforts is required to compensate the dead zones by modifying PWM modulation strategy. Recently, there are three main types of phase current reconstruction [30], [31].

A phase-shifted FTC is proposed for single phase current control, in which the good control results has been achieved, but there is a problem of difficulty in adjusting the parameters of the PI regulator [32]. Aiming at the sensorless control of single current sensor, the method of injecting high-frequency voltage is used to reduce the error of the reconstructed current, and the relevant experimental verification is carried out [26]. As we all know, there is the blind spot of current reconstruction which has been researched widely by scholars at home and abroad when SVPWM control is applied [33], [34], [35]. In [36], injecting square waves based on the d-axis voltage of the rotor is adopted to reduce the harmonic components of the reconstructed current, so the control performance of the system is significantly improved. In [37], changing the circuit topology is applied, and at the same time the cost and volume of the hardware circuit must be increased.

In view of all mentioned above, the DTFC used for the look-up-table-based DTFC is proposed based on the series-phase effect and different phase principle of DC-link current without adding hardware circuit and parameters in this paper. In addition, the proposed DTFC of PPMLM is not only limited to long-distance transportation systems, but can also be applied to other application engineering fields for robot, vehicle or flight control such as [38], [39].

This paper is organized as follows. The studied PPMLM system is described in Section II. In Section III, the proposed DTFC (P-DTFC) are introduced exhaustively and simulation analysis is implemented in Section IV. Experiments are carried out in Section V to verify the theoretical analysis. Finally, conclusions are drawn in Section V.

## II. STUDIED PPMLM SYSTEM

### A. THE TOPOLOGY OF PPMLM SYSTEM

The topology of PPMLM system is shown in Figure 1, where VSI is a three-phase voltage inverter; $i_a$, $i_b$, and $i_c$ are the current of PPMLM; meanwhile $u_{dc}$ and $i_{dc}$ are the DC-link voltage and current of PPMLM system, respectively.

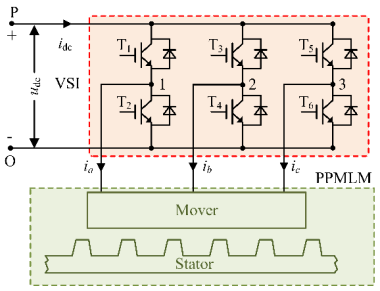


**FIGURE 1.** The topology of PPMLM system.

### B. PPMLM

In Figure 2, the structure of PPMLM is displayed. In the mover, where two coils serially are consisted in phase winding and separated by a magnetic barrier, while a magnetic barrier is also placed between the different phases, the PM and armature winding are all installed in the primary (mover) while the silicon steel sheets is only included in the secondary (stator). The structure of E-module is shown in Figure 3, the value of parameters are depicted in Section V in detail.

The $dq$ axis of PPMLM is defined as shown in Figure 4. The position where the phase-A PM flux linkage of PPMLM is maximum is $d$ axis, while the $q$ axis is 90° ahead of $d$ axis by an electrical angle (i.e. the front quarter stator pole pitch $\tau_s$).

So, the voltage-current balance equation of PPMLM is described as:

$$\begin{cases} u_d = R_s i_d + L_s \dfrac{di_d}{dt} - \dfrac{2\pi v}{\tau_s} L_s i_q \\ u_q = R_s i_q + L_s \dfrac{di_q}{dt} + \dfrac{2\pi v}{\tau_s}(\psi_m + L_s i_d) \end{cases} \tag{1}$$

where $u_d$, $u_q$ are $dq$-axis voltage, $i_d$, $i_q$ are $dq$-axis current. $R_s$, $L_s$, $\psi_m$ are stator resistance, inductance and PM flux linkage respectively. $v$ is speed of mover. $\tau_s$ is the stator pole pitch.

## III. PROPOSED DTFC

In this section, the P-DTFC which is derived from the traditional DTFC (T-DTFC) and equivalent DTFC (E-DTFC) is described in detail, so the T-DTFC is firstly introduced.

### A. T-DTFC

The switching state $s_x$ of bridge $x$ is defined as:

$$s_x = \begin{cases} 1 & \text{upper bridge is on} \\ 0 & \text{upper bridge is off} \end{cases} \quad (x = 1, 2, 3) \tag{2}$$

Considering the different switch states, there are 8 voltage vectors in the VSI inverter which consist of 2 zero voltage vectors and 6 active voltage vectors (AVVs).

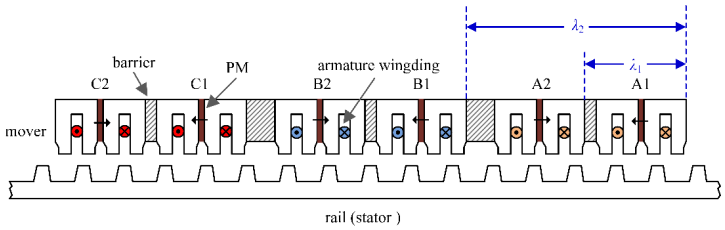


**FIGURE 2.** The structure of PPMLM.

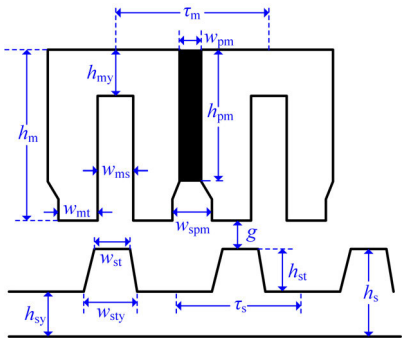


**FIGURE 3.** The structure of E-type module.

In PPMLM system, the voltage-integral flux observer is adopted in the T-DTFC.

$$\boldsymbol{\psi} = \int (\boldsymbol{u} - R_s \boldsymbol{i}) dt + \boldsymbol{\psi}_0 \tag{3}$$

With $\boldsymbol{\psi} = \begin{bmatrix} \psi_\alpha \\ \psi_\beta \end{bmatrix}$, $\boldsymbol{u} = \begin{bmatrix} u_\alpha \\ u_\beta \end{bmatrix}$, $\boldsymbol{i} = \begin{bmatrix} i_\alpha \\ i_\beta \end{bmatrix}$, $\boldsymbol{\psi}_0 = \begin{bmatrix} \psi_{\alpha 0} \\ \psi_{\beta 0} \end{bmatrix}$. where, $i_\alpha$, $i_\beta$, $u_\alpha$, $u_\beta$, $\psi_\alpha$, $\psi_\beta$, $\psi_{\alpha 0}$, $\psi_{\beta 0}$ are current, voltage, flux linkage and initial PM flux linkage of PPMLM in $\alpha\beta$ axis system.

The amplitude and angle of flux linkage are expressed by formula (4) as

$$\begin{cases} \psi_s = \sqrt{\psi_\alpha^2 + \psi_\beta^2} \\ \theta_s = \arctan(\psi_\beta / \psi_\alpha) \end{cases} \tag{4}$$

While the thrust force $F_e$ is calculated by

$$F_e = \frac{3\pi}{\tau_s}(\psi_\alpha i_\beta - \psi_\beta i_\alpha) \tag{5}$$

The bang-bang control is used to get the thrust force instruction $\sigma_F$ and flux linkage instruction $\sigma_\psi$ by

$$\sigma_F = \begin{cases} 1 & (e_F > H_F) \\ 0 & (e_F < -H_F) \end{cases} \quad (e_F = F_e^* - F_e) \tag{6}$$

$$\sigma_\psi = \begin{cases} 1 & (e_\psi > H_\psi) \\ 0 & (e_\psi < -H_\psi) \end{cases} \quad (e_\psi = \psi^* - \psi_s) \tag{7}$$

where $H_F$ and $H_\psi$ are the thrust force and flux linkage band width, respectively.

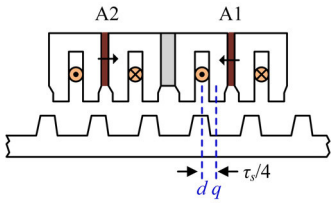


**FIGURE 4.** Definition of dq-axis for PPMLM.

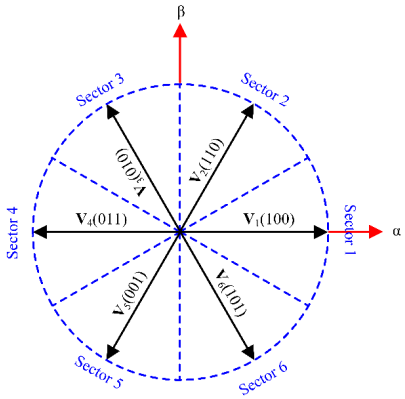


**FIGURE 5.** The space distribution of AVVs and sector.

Flux sector $N$ is defined as

$$\pi(2N-3)/6 <= N < \pi(2N-1)/6, \quad N = 1, 2, 3, 4, 5, 6 \tag{8}$$

The space distribution of AVVs and flux linkage sector are shown in Figure 5.

The sector $N$ can be determined where the flux linkage is located by flux linkage angle $\theta_s$ and formula (6).

According to $\sigma_F$, $\sigma_\psi$ and sector $N$, the AVV is selected from Table 1 and implemented to the driving of PPMLM system.

### B. E-DTFC

It can be known from the space voltage vector distribution and geometric knowledge that any AVV (such as $\mathbf{V}_1$) is equal to the sum of its adjacent two AVVs (such as $\mathbf{V}_2$, $\mathbf{V}_6$), which is called the principle of equivalent voltage vector in this paper. Then, the any AVV (such as $\mathbf{V}_1$) before equivalent is defined

**TABLE 1.** The selection principle of AVVs.

| | $\sigma_\psi$=1 | | $\sigma_\psi$=0 | |
|---|---|---|---|---|
| | $\sigma_F$=1 | $\sigma_F$=0 | $\sigma_F$=1 | $\sigma_F$=0 |
| Sector 1 | $V_2(110)$ | $V_6(101)$ | $V_3(010)$ | $V_5(001)$ |
| Sector 2 | $V_3(010)$ | $V_1(100)$ | $V_4(011)$ | $V_6(101)$ |
| Sector 3 | $V_4(011)$ | $V_2(110)$ | $V_5(001)$ | $V_1(100)$ |
| Sector 4 | $V_5(001)$ | $V_3(010)$ | $V_6(101)$ | $V_2(110)$ |
| Sector 5 | $V_6(101)$ | $V_4(011)$ | $V_1(100)$ | $V_3(010)$ |
| Sector 6 | $V_1(100)$ | $V_5(001)$ | $V_2(110)$ | $V_4(011)$ |

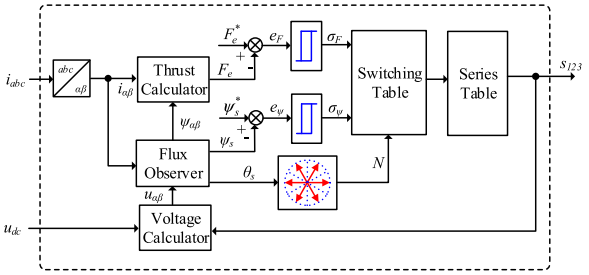


**FIGURE 6.** The control block diagram of E-DTFC.

as the basic voltage vector (BVV), meanwhile the adjacent two AVVs (such as $\mathbf{V}_2$, $\mathbf{V}_6$) after equivalent are defined as the sub-basic voltage vector (SBVV).

For the convenience of expression, the SBVV are added an underline $\underline{\mathbf{V}}_n$ $(n = 1, 2, \cdots, 6)$ in this paper, when the BVV is not with an underline. So the principle of equivalent voltage vector is shown in Equation (9).

$$\begin{cases} \mathbf{V}_1 = \underline{\mathbf{V}}_2 + \underline{\mathbf{V}}_6 \quad \mathbf{V}_2 = \underline{\mathbf{V}}_1 + \underline{\mathbf{V}}_3 \quad \mathbf{V}_3 = \underline{\mathbf{V}}_2 + \underline{\mathbf{V}}_4 \\ \mathbf{V}_4 = \underline{\mathbf{V}}_3 + \underline{\mathbf{V}}_5 \quad \mathbf{V}_5 = \underline{\mathbf{V}}_4 + \underline{\mathbf{V}}_6 \quad \mathbf{V}_6 = \underline{\mathbf{V}}_1 + \underline{\mathbf{V}}_5 \end{cases} \tag{9}$$

According to the principle of volt-second balance, equation (9) can be expressed as

$$\begin{cases} \mathbf{V}_1 \times T_{\mathbf{sc}} = \underline{\mathbf{V}}_2 \times T_{\mathbf{sc}} + \underline{\mathbf{V}}_6 \times T_{\mathbf{sc}} \\ \mathbf{V}_2 \times T_{\mathbf{sc}} = \underline{\mathbf{V}}_1 \times T_{\mathbf{sc}} + \underline{\mathbf{V}}_3 \times T_{\mathbf{sc}} \\ \mathbf{V}_3 \times T_{\mathbf{sc}} = \underline{\mathbf{V}}_2 \times T_{\mathbf{sc}} + \underline{\mathbf{V}}_4 \times T_{\mathbf{sc}} \\ \mathbf{V}_4 \times T_{\mathbf{sc}} = \underline{\mathbf{V}}_3 \times T_{\mathbf{sc}} + \underline{\mathbf{V}}_5 \times T_{\mathbf{sc}} \\ \mathbf{V}_5 \times T_{\mathbf{sc}} = \underline{\mathbf{V}}_4 \times T_{\mathbf{sc}} + \underline{\mathbf{V}}_6 \times T_{\mathbf{sc}} \\ \mathbf{V}_6 \times T_{\mathbf{sc}} = \underline{\mathbf{V}}_1 \times T_{\mathbf{sc}} + \underline{\mathbf{V}}_5 \times T_{\mathbf{sc}} \end{cases} \tag{10}$$

where, $T_{\mathrm{sc}}$ is the sampling period.

Therefore, according to the principle of equivalent voltage vector, that is, equation (10), the equivalent DTFC (E-DTFC) in which two consecutive sampling periods are seen as a control period is proposed in this paper. While the BVV obtained by T-DTFC is equivalent to the two SBVV, which are continuously outputted in the two consecutive sampling periods.

The control block diagram of E-DTFC is shown as Figure 6. What needs to be pointed out here is that the output SBVV sequence has almost no effect on the control result of PPMLM, which is different from the proposed DTFC (P-DTFC) later in the next part.

**TABLE 2.** The series phenomenon of the DC–link current.

| AVVs | series phenomenon |
|---|---|
| $V_1(100)$ | $i_a$=$i_{dc}$ |
| $V_2(110)$ | $i_c$=-$i_{dc}$ |
| $V_3(010)$ | $i_b$=$i_{dc}$ |
| $V_4(011)$ | $i_a$=-$i_{dc}$ |
| $V_5(001)$ | $i_c$=$i_{dc}$ |
| $V_6(101)$ | $i_b$=-$i_{dc}$ |

### C. P-DTFC

#### 1) THE SERIES PHENOMENON OF DC-LINK CURRENT

The positive direction of the current sensor measurement is defined as shown by the arrow direction in Figure 1. The DC-link current will be connected in series with one of the three phases, when any AVV is outputted by the VSI inverter, so the DC–link current is equal to or opposite to the current of the series-connected phase in value, which is referred to in this paper as the series phenomenon of the DC–link current. The series phenomenon of the DC–link current is shown in Table 2. In order to ensure the accuracy of the reconstructed current, only the AVV is used in the DTFC control in this paper. Therefore, the problem of measurement dead zone of the current reconstruction at this time is not existed because the measurement time is long enough.

#### 2) THE PRINCIPLE OF DIFFERENT PHASE MODE

Obviously, the current measured in one control cycle which consists of two sampling periods may be in the same phase, when the E-DTFC is applied in the PPMLM drive system. Which will lead to the larger current error between the measured and reconstructed currents. So the principle of different phase mode in which the information of current is updated different from the previous sampling period is proposed, meanwhile the two phases can be measured in one control cycle and the third current can be calculated by the sum of three phases is zero, which can ensure that the error between the measured and reconstructed currents is strictly limited in one sampling period delay.

According to the current BVV and the current information of the previous sampling period, it can be known that there are 18 cases, as shown in Table 3. Clearly, in the 1st, 6th, 8th, 10th, 15th, and 17th cases, no matter the output sequence of the SBVV, the accuracy of the reconstructed current will not be affected.

Therefore, combined with the E-DTFC and different phase mode, the P-DTFC control under the condition of a single DC-link current sensor is realized, while the effective control of the PPMLM system can be completed.

The P-DTFC control block diagram is shown in Figure 7.

## IV. PERFORMANCE ANALYSIS

In this part, several simulations are carried on based on MATLAB in order to verify the correctness of P-DTFC, and E-DTFC is also simulated as a comparison. The simulation parameter is listed in Table 4.

**TABLE 3.** The principle of different phase mode.

| Case | BVV | Current information | Output sequence | |
|---|---|---|---|---|
| 1 | $\mathbf{V}_1(100)$ | phase A | $\underline{\mathbf{V}}_2(110)/\underline{\mathbf{V}}_6(101)$ | $\underline{\mathbf{V}}_6(101)/\underline{\mathbf{V}}_2(110)$ |
| 2 | $\mathbf{V}_1(100)$ | phase B | $\underline{\mathbf{V}}_2(110)$ | $\underline{\mathbf{V}}_6(101)$ |
| 3 | $\mathbf{V}_1(100)$ | phase C | $\underline{\mathbf{V}}_6(101)$ | $\underline{\mathbf{V}}_2(110)$ |
| 4 | $\mathbf{V}_2(110)$ | phase A | $\underline{\mathbf{V}}_3(010)$ | $\underline{\mathbf{V}}_1(100)$ |
| 5 | $\mathbf{V}_2(110)$ | phase B | $\underline{\mathbf{V}}_1(100)$ | $\underline{\mathbf{V}}_3(010)$ |
| 6 | $\mathbf{V}_2(110)$ | phase C | $\underline{\mathbf{V}}_3(010)/\underline{\mathbf{V}}_1(100)$ | $\underline{\mathbf{V}}_1(100)/\underline{\mathbf{V}}_3(010)$ |
| 7 | $\mathbf{V}_3(010)$ | phase A | $\underline{\mathbf{V}}_2(110)$ | $\underline{\mathbf{V}}_4(011)$ |
| 8 | $\mathbf{V}_3(010)$ | phase B | $\underline{\mathbf{V}}_4(011)/\underline{\mathbf{V}}_2(110)$ | $\underline{\mathbf{V}}_2(110)/\underline{\mathbf{V}}_4(011)$ |
| 9 | $\mathbf{V}_3(010)$ | phase C | $\underline{\mathbf{V}}_4(011)$ | $\underline{\mathbf{V}}_2(110)$ |
| 10 | $\mathbf{V}_4(011)$ | phase A | $\underline{\mathbf{V}}_3(010)/\underline{\mathbf{V}}_5(001)$ | $\underline{\mathbf{V}}_5(001)/\underline{\mathbf{V}}_3(010)$ |
| 11 | $\mathbf{V}_4(011)$ | phase B | $\underline{\mathbf{V}}_5(001)$ | $\underline{\mathbf{V}}_3(010)$ |
| 12 | $\mathbf{V}_4(011)$ | phase C | $\underline{\mathbf{V}}_3(010)$ | $\underline{\mathbf{V}}_5(001)$ |
| 13 | $\mathbf{V}_5(001)$ | phase A | $\underline{\mathbf{V}}_6(101)$ | $\underline{\mathbf{V}}_4(011)$ |
| 14 | $\mathbf{V}_5(001)$ | phase B | $\underline{\mathbf{V}}_4(011)$ | $\underline{\mathbf{V}}_6(101)$ |
| 15 | $\mathbf{V}_5(001)$ | phase C | $\underline{\mathbf{V}}_6(101)/\underline{\mathbf{V}}_4(011)$ | $\underline{\mathbf{V}}_4(011)/\underline{\mathbf{V}}_6(101)$ |
| 16 | $\mathbf{V}_6(101)$ | phase A | $\underline{\mathbf{V}}_5(001)$ | $\underline{\mathbf{V}}_1(100)$ |
| 17 | $\mathbf{V}_6(101)$ | phase B | $\underline{\mathbf{V}}_5(001)/\underline{\mathbf{V}}_1(100)$ | $\underline{\mathbf{V}}_1(100)/\underline{\mathbf{V}}_5(001)$ |
| 18 | $\mathbf{V}_6(101)$ | phase B | $\underline{\mathbf{V}}_1(100)$ | $\underline{\mathbf{V}}_5(001)$ |

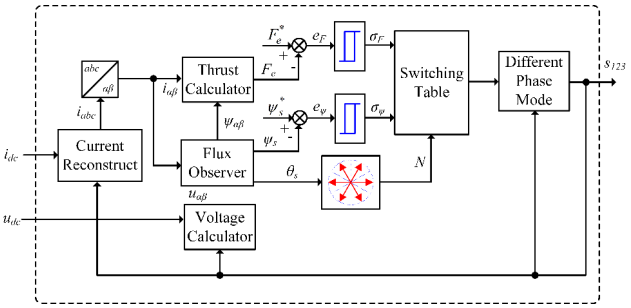


**FIGURE 7.** The control block diagram of P-DTFC.

**TABLE 4.** The parameters of simulation.

| Parameter | Value |
|---|---|
| DC-link voltage, $u_{dc}$ (V) | 50 |
| Simulation step, $T_s$(s) | 1E-6 |
| Sampling period, $T_{sc}$(s) | 5E-5 |
| Stator inductance, $L_s$(mH) | 32.5 |
| Stator resistance, $R_s(\Omega)$ | 3.3 |
| PM flux linkage, $\psi_s$(Wb) | 0.165 |
| Rated thrust, $F_e$(N) | 150 |
| Friction coefficient, $D$(kg/s) | 0.004 |
| Mover mass, $M$(kg) | 32.6 |

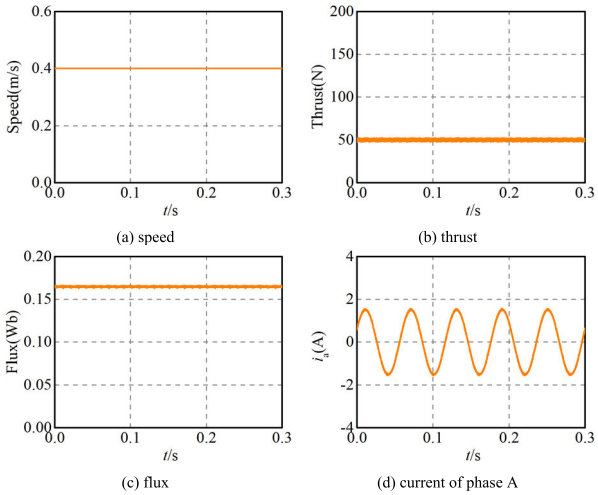


**FIGURE 8.** Steady-state simulation performance of E-DTFC.

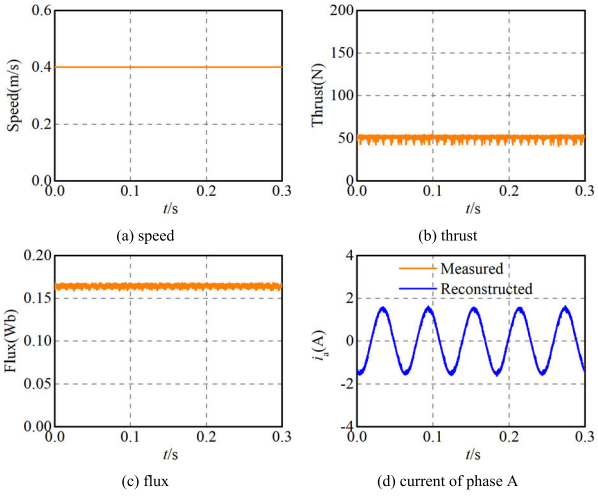


**FIGURE 9.** Steady-state simulation performance of P-DTFC.

### A. STEADY-STATE PERFORMANCE OF SIMULATION

To analyze the steady-state performance of P-DTFC and E-DTFC, the reference speed is 0.4 m/s and the load is set as 50 N. The simulation results are shown in Figure 8 and Figure 9.

As the Figure 8 and Figure 9 shown that both DTFC can accomplish good steady-state performance in which the speed, thrust and flux of PPMLM can track the reference value well with less fluctuation. The current waveform of phase A is close to sinusoidal without harmonic content. Meanwhile, in P-DTFC the current error of phase A between the measured current and the reconstructed current is nearly zero, which can prove the correctness of previous analysis in Section III.

### B. THRUST RESPONSE OF SIMULATION

For verifying the thrust response simulation performance of P-DTFC and E-DTFC, this simulation is carried out, which the given thrust increases from −120 N to 120 N, while the speed regulator can be ignored. The simulation results are exhibited in Figure 10.

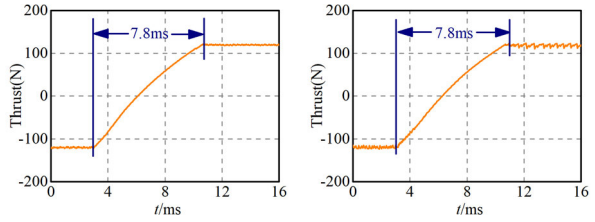


**FIGURE 10.** The response of thrust of simulation.

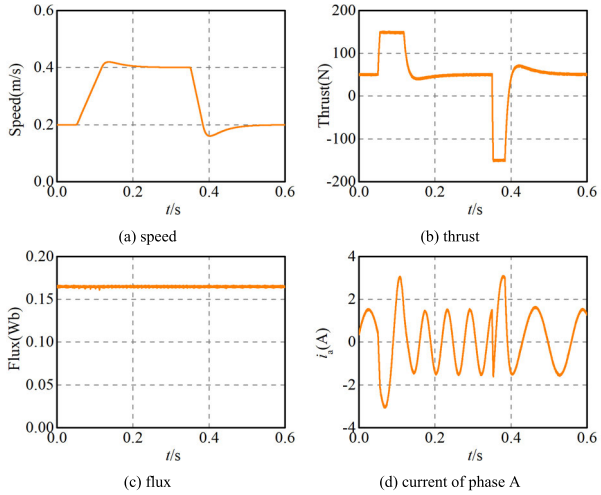


**FIGURE 11.** Speed response simulation performance of E-DTFC.

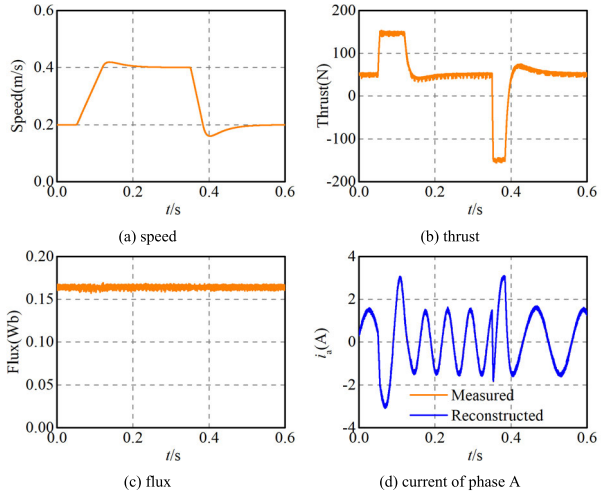


**FIGURE 12.** Speed response simulation performance of P-DTFC.

As is depicted in Figure 10 that both DTFC have the same thrust response, while both the thrust response of simulation is 7.8 ms.

### C. SPEED RESPONSE OF SIMULATION

To test the speed response simulation performance of the P-DTFC and E-DTFC, the reference speed increases from 0.2 m/s to 0.4 m/s, then recovers to 0.2 m/s, while the load is set as 50 N. The simulation results are illustrated in Figure 11 and Figure 12.

**TABLE 5.** The parameters of PPMLM.

| Parameter | Value |
|---|---|
| Mover width, $w_m$ (mm) | 160 |
| Mover pole pitch, $\tau_m$ (mm) | 26 |
| Stator pole pitch, $\tau_s$ (mm) | 24 |
| Mover tooth width, $w_{mt}$ (mm) | $\tau_m/4$ |
| Mover slot mouth width, $w_{msm}$(mm) | $\tau_m/4$ |
| Mover slot width, $w_{ms}$ (mm) | $\tau_m/4$ |
| Slot width (Under PM), $w_{ms}$ (mm) | $\tau_m/4$ |
| Mover height, $h_m$ (mm) | 35 |
| Mover yoke height, $h_{my}$ (mm) | 10 |
| Magnet height, $h_{pm}$ (mm) | $0.9*h_m$ |
| Magnet width, $w_{pm}$ (mm) | 5 |
| Air gap length, $g$ (mm) | 2 |
| Stator tooth width, $w_{st}$ (mm) | $1.6*\tau_m/4$ |
| Stator teeth yoke width, $w_{sty}$ (mm) | $2*\tau_m/4$ |
| Stator tooth height, $h_{st}$ (mm) | 10 |
| Stator yoke height, $h_{sy}$ (mm) | 13 |
| Stator height, $h_s$ (mm) | 23 |
| Coil spacing, $\lambda_1$ (mm) | $(2+1/2)*\tau_s$ |
| Phase spacing, $\lambda_2$ (mm) | $(5+1/3)*\tau_s$ |
| Number of turns per coil, $N_{coil}$ | 114 |
| Phase resistance (Ω), $R_s$ | 3 |
| Stack factor | 0.95 |
| Rate current $I_{rms}$ (A) | 3 |
| Rated speed (m/s) | 1.2 |
| Maximum load (N) | 150 |

It is shown that the given speed is tracked well, while the flux linkage can maintain 0.165 Wb despite the change of speed. Similarly, the current error of phase A can be neglected.

## V. EXPERIMENTAL VALIDATION

To verify the feasibility and accuracy of P-DTFC, the PPMLM system is established based on dSPACE DS1103 controller, as shown in Figure 13. In which the DC-link voltage is set as 50 V, while the sampling period is set as 50 ms. The PPMLM parameters are shown in Table 5. The steady-state and dynamic-state experiments of P-DTFC are carried out. In addition, several experiments for E-DTFC are also implemented as a comparison.

### A. STEADY-STATE PERFORMANCE OF EXPERIMENT

This experiment is to verify the steady-state performance of P-DTFC and E-DTFC. The given speed is set as 0.4 m/s and the load is 50 N. The experimental results are shown in Figure 14 and Figure 15.

As can be seen from Figure 14 and Figure 15 that the speed is fluctuated around at 0.4 m/s and the thrust force is equal to 50 N approximately in both DTFC since the friction coefficient between mover and stator is variable in different location. The flux linkage is always maintain the constant for each DTFC. Furthermore, the waveforms of the reconstructed current and the measured current are almost coincident in P-DTFC, which is caused by the temperature drift effect of the sampling circuit.

### B. THRUST RESPONSE OF EXPERIMENT

To compare the thrust response performance of P-DTFC and E-DTFC, the reference thrust force increases from −120 N to 120 N, in which the effect of PI regulator can be neglected. The experimental results are demonstrated in Figure 16.

It can be found that the thrust response of E-DTFC and P-DTFC is 12.3 ms and 11.6 ms respectively. Which can be

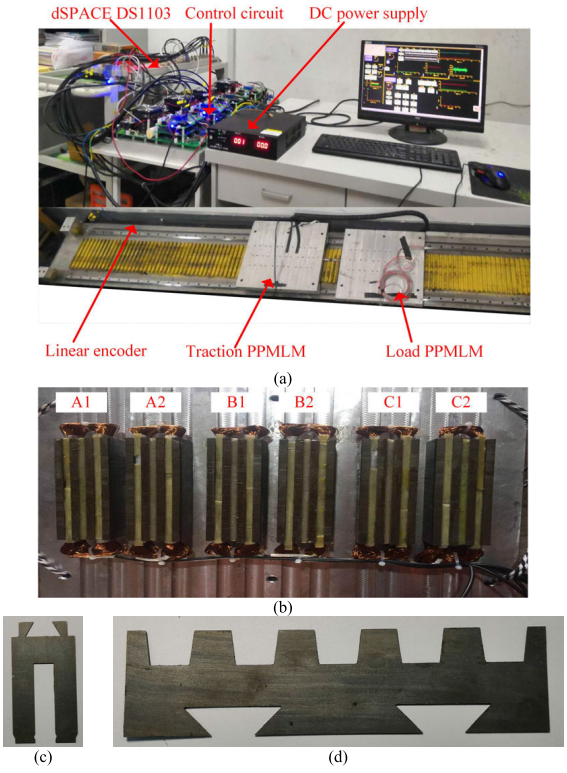


**FIGURE 13.** Experiment platform: (a) entire view, (b) bottom view of mover, (c) mover teeth (d) stator (rail) teeth.

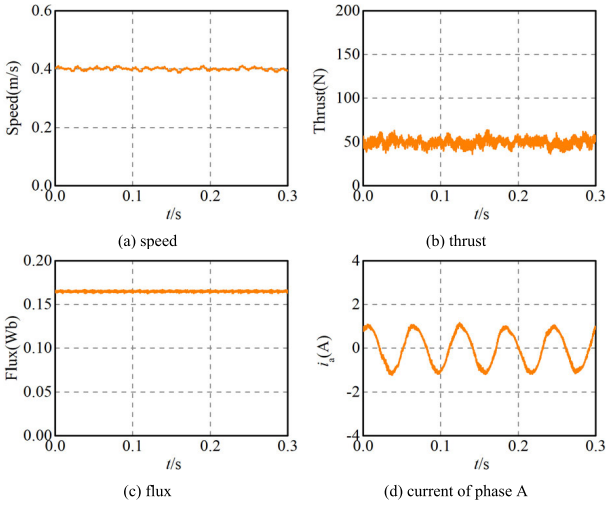


**FIGURE 14.** Steady-state experiment performance of E-DTFC.

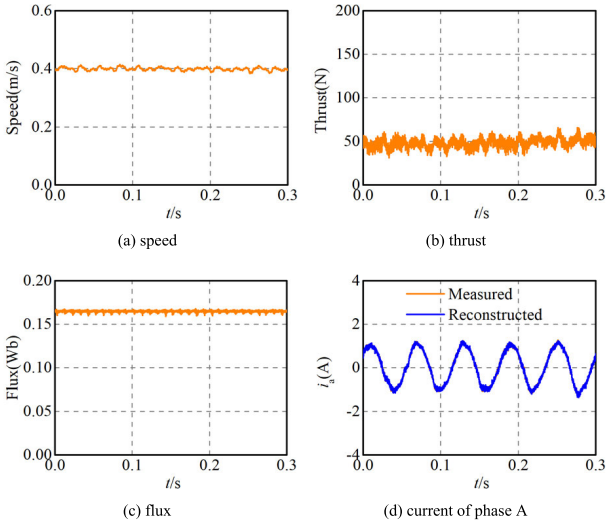


**FIGURE 15.** Steady-state experiment performance of P-DTFC.

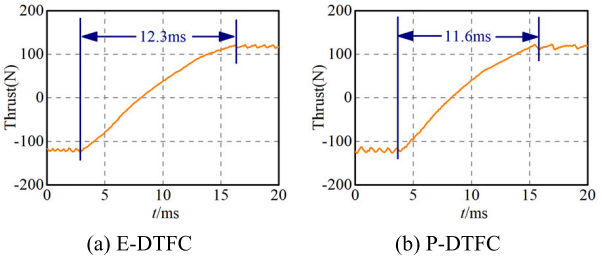


**FIGURE 16.** The response of thrust of experiment.

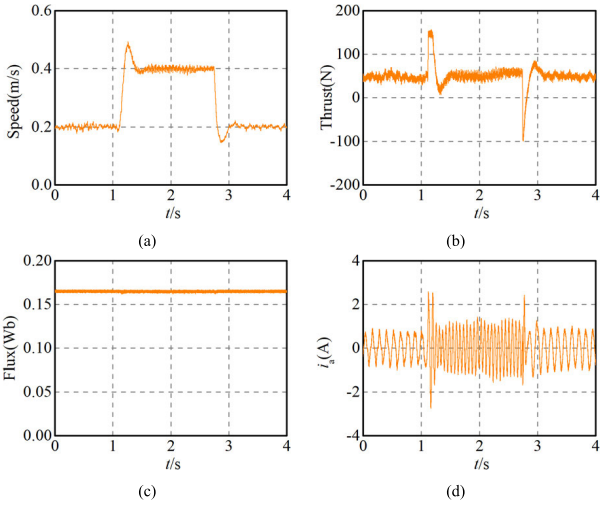


**FIGURE 17.** Speed response experiment performance of E-DTFC: (a) speed, (b) thrust, (c) flux (d) phase current.

seen as both DTFC have the same thrust response, although only a single DC-link current sensor is used in P-DTFC.

### C. SPEED RESPONSE OF EXPERIMENT

This experiment is to verify the speed response of P-DTFC and E-DTFC. The reference speed increases from 0.2 m/s to 0.4 m/s, then decreases to 0.2 m/s. The experimental results are illustrated in Figure 17 and Figure 18.

Both P-DTFC and T-DTFC can demonstrate good speed response performance. The flux linkage maintains constant value at about 0.165 Wb despite of the variable speed. In Figure 18, similarly with simulation analysis, the current error of phase A can also be ignored.

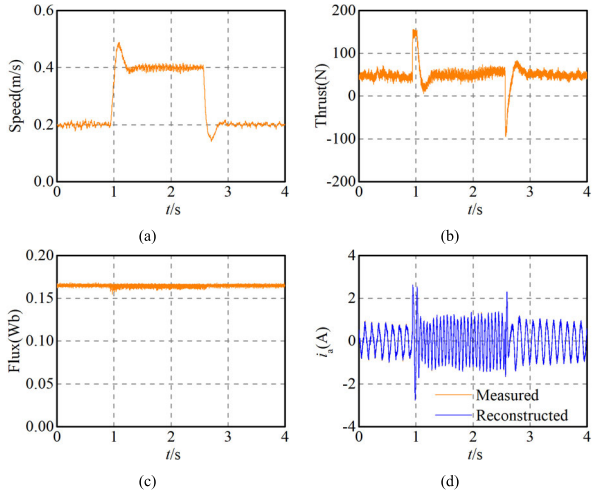


**FIGURE 18.** Speed response experiment performance of P-DTFC: (a) speed, (b) thrust, (c) flux (d) phase current.

## VI. CONCLUSION

In this paper, the P-DTFC of PPMLM system is proposed to enhance the FTC ability of the current sensor of PPMLM drive system. In P-DTFC, only one current sensor and one voltage sensor is applied, the parameter resistance is needed which can be seen as constant. Furthermore, the linear encoder can be removed from the P-DTFC strategy because of the electrical angle is not used. Meanwhile, compare with E-DTFC, the P-DTFC can keep the same steady-state and dynamic-state performance with a single DC-link current sensor. And the P-DTFC is verified through the simulation and experimental results.

## REFERENCES

[1] W. Wang, W. Tian, Z. Wang, W. Hua, and M. Cheng, "A fault diagnosis method for current sensors of primary permanent-magnet linear motor drives," *IEEE Trans. Power Electron.*, vol. 36, no. 2, pp. 2334–2345, Feb. 2021.

[2] Q. Yu, W. Wang, Y. Feng, W. Tian, and Q. Shen, "Direct thrust force control of half-open winding primary permanent magnet linear motor," *IEEE Access*, vol. 10, pp. 59970–59978, 2022.

[3] W. Xu, X. Xiao, G. Du, D. Hu, and J. Zou, "Comprehensive efficiency optimization of linear induction motors for urban transit," *IEEE Trans. Veh. Technol.*, vol. 69, no. 1, pp. 131–139, Jan. 2020.

[4] Q. Wang, Y. Chen, Y. Guo, J. Zhang, and Y. Li, "Performance modeling and analysis of a doubly yokeless permanent magnet linear motor with improved thrust force quality," *IEEE Access*, vol. 7, pp. 160586–160594, 2019.

[5] X. Liu, S. Zhen, H. Zhao, H. Sun, and Y.-H. Chen, "Fuzzy-set theory based optimal robust design for position tracking control of permanent magnet linear motor," *IEEE Access*, vol. 7, pp. 153829–153841, 2019.

[6] Y. Sui, Z. Yin, M. Wang, B. Yu, and P. Zheng, "A tubular staggered-teeth transverse-flux PMLM with circumferentially distributed three-phase windings," *IEEE Trans. Ind. Electron.*, vol. 66, no. 6, pp. 4837–4848, Jun. 2019.

[7] X. Yang, W. Zhao, and B. Song, "Thrust force calculation and analysis for the permanent magnet linear motor motion system considering the encoder errors," *IEEE Trans. Ind. Electron.*, vol. 69, no. 6, pp. 6069–6079, Jun. 2022.

[8] Q. Wang, Y. Yang, P. Ma, J. Zhang, and Y. Li, "Analysis and suppression of phase unbalance induced force ripples in permanent magnet linear motors," *IEEE Access*, vol. 10, pp. 5416–5423, 2022.

[9] J. Liu, J. Cao, Z. Cheng, and L. Li, "Study on the position estimation method of winding segmented permanent magnet linear motor," *IEEE Access*, vol. 10, pp. 51242–51248, 2022.

[10] R. Cao, M. Cheng, and W. Hua, "Investigation and general design principle of a new series of complementary and modular linear FSPM motors," *IEEE Trans. Ind. Electron.*, vol. 60, no. 12, pp. 5436–5446, Dec. 2013, doi: 10.1109/TIE.2012.2230605.

[11] W. Wang, Z. Lu, W. Tian, W. Hua, Z. Wang, and M. Cheng, "Dual-vector located model predictive control with single DC-link current sensor for permanent-magnet linear motor drives," *IEEE Trans. Power Electron.*, vol. 36, no. 12, pp. 14142–14154, Dec. 2021, doi: 10.1109/TPEL.2021.3093546.

[12] R. Cao, N. Jiang, and M. Lu, "Sensorless control of linear flux-switching permanent magnet motor based on extended Kalman filter," *IEEE Trans. Ind. Electron.*, vol. 67, no. 7, pp. 5971–5979, Jul. 2020.

[13] X. Lin, W. Huang, W. Jiang, Y. Zhao, and S. Zhu, "Deadbeat direct torque and flux control for permanent magnet synchronous motor based on stator flux oriented," *IEEE Trans. Power Electron.*, vol. 35, no. 5, pp. 5078–5092, May 2020.

[14] W. Zhao, B. Wu, Q. Chen, and J. Zhu, "Fault-tolerant direct thrust force control for a dual inverter fed open-end winding linear Vernier permanent-magnet motor using improved SVPWM," *IEEE Trans. Ind. Electron.*, vol. 65, no. 9, pp. 7458–7467, Sep. 2018.

[15] W. Wang, Y. Feng, Y. Shi, M. Cheng, W. Hua, and Z. Wang, "Direct thrust force control of primary permanent-magnet linear motors with single DC-link current sensor for subway applications," *IEEE Trans. Power Electron.*, vol. 35, no. 2, pp. 1365–1376, Feb. 2020.

[16] Y. Zuo, J. Mei, C. Jiang, and C. H. T. Lee, "Digital implementation of deadbeat-direct torque and flux control for permanent magnet synchronous machines in the *M–T* reference frame," *IEEE Trans. Power Electron.*, vol. 36, no. 4, pp. 4610–4621, Apr. 2021.

[17] W. Zhao, A. Yang, J. Ji, Q. Chen, and J. Zhu, "Modified flux linkage observer for sensorless direct thrust force control of linear Vernier permanent magnet motor," *IEEE Trans. Power Electron.*, vol. 34, no. 8, pp. 7800–7811, Aug. 2019.

[18] W. Wang, C. Liu, H. Zhao, and Z. Song, "Improved deadbeat-direct torque and flux control for PMSM with less computation and enhanced robustness," *IEEE Trans. Ind. Electron.*, early access, May 3, 2022, doi: 10.1109/TIE.2022.3170619.

[19] W. Wang, Y. Feng, Y. Shi, M. Cheng, W. Hua, and Z. Wang, "Fault-tolerant control of primary permanent-magnet linear motors with single phase current sensor for subway applications," *IEEE Trans. Power Electron.*, vol. 34, no. 11, pp. 10546–10556, Nov. 2019, doi: 10.1109/TPEL.2019.2899168.

[20] M. Khayamy and H. Chaoui, "Current sensorless MTPA operation of interior PMSM drives for vehicular applications," *IEEE Trans. Veh. Technol.*, vol. 67, no. 8, pp. 6872–6881, Aug. 2018, doi: 10.1109/TVT.2018.2823538.

[21] B. Cai, Y. Liu, and M. Xie, "A dynamic-Bayesian-network-based fault diagnosis methodology considering transient and intermittent faults," *IEEE Trans. Autom. Sci. Eng.*, vol. 14, no. 1, pp. 276–285, Jan. 2017.

[22] X. Kong, B. Cai, Y. Liu, H. Zhu, Y. Liu, H. Shao, C. Yang, H. Li, and T. Mo, "Optimal sensor placement methodology of hydraulic control system for fault diagnosis," *Mech. Syst. Signal Process.*, vol. 174, Jul. 2022, Art. no. 109069.

[23] B. Cai, K. Hao, Z. Wang, C. Yang, X. Kong, Z. Liu, R. Ji, and Y. Liu, "Data-driven early fault diagnostic methodology of permanent magnet synchronous motor," *Expert Syst. Appl.*, vol. 177, Sep. 2021, Art. no. 115000.

[24] J. Lu, X. Zhang, Y. Hu, J. Liu, C. Gan, and Z. Wang, "Independent phase current reconstruction strategy for IPMSM sensorless control without using null switching states," *IEEE Trans. Ind. Electron.*, vol. 65, no. 6, pp. 4492–4502, Jun. 2018.

[25] S. Xiao, T. Shi, X. Li, Z. Wang, and C. Xia, "Single-current-sensor control for PMSM driven by quasi-Z-source inverter," *IEEE Trans. Power Electron.*, vol. 34, no. 7, pp. 7013–7024, Jul. 2019.

[26] J. Zhao, S. Nalakath, and A. Emadi, "A high frequency injection technique with modified current reconstruction for low-speed sensorless control of IPMSMs with a single DC-link current sensor," *IEEE Access*, vol. 7, pp. 136137–136147, 2019, doi: 10.1109/ACCESS.2019.2942148.

[27] Y. Cho, T. LaBella, and J.-S. Lai, "A three-phase current reconstruction strategy with online current offset compensation using a single current sensor," *IEEE Trans. Ind. Electron.*, vol. 59, no. 7, pp. 2924–2933, Jul. 2012, doi: 10.1109/TIE.2011.2171177.

[28] H. Kim and T. M. Jahns, "Current control for AC motor drives using a single DC-link current sensor and measurement voltage vectors," *IEEE Trans. Ind. Appl.*, vol. 42, no. 6, pp. 1539–1547, Nov./Dec. 2006, doi: 10.1109/TIA.2006.882630.
[29] H.-C. Chen, C.-Y. Lu, and L.-M. Huang, "Decoupled current-balancing control with single-sensor sampling-current strategy for two-phase interleaved boost-type converters," *IEEE Trans. Ind. Electron.*, vol. 63, no. 3, pp. 1507–1518, Mar. 2016, doi: 10.1109/TIE.2015.2498135.
[30] W. Wang, Z. Lu, Y. Feng, W. Tian, W. Hua, Z. Wang, and M. Cheng, "Coupled fault-tolerant control of primary permanent-magnet linear motor traction systems for subway applications," *IEEE Trans. Power Electron.*, vol. 36, no. 3, pp. 3408–3421, Mar. 2021, doi: 10.1109/TPEL.2020.3015519.
[31] M. Manohar and S. Das, "Current sensor fault-tolerant control for direct torque control of induction motor drive using flux-linkage observer," *IEEE Trans. Ind. Informat.*, vol. 13, no. 6, pp. 2824–2833, Dec. 2017.
[32] W. Wang, X. Zeng, W. Hua, Z. Wang, and M. Cheng, "Phase-shifting fault-tolerant control of permanent-magnet linear motors with single-phase current sensor," *IEEE Trans. Ind. Electron.*, vol. 69, no. 3, pp. 2414–2425, Mar. 2022, doi: 10.1109/TIE.2021.3068552.
[33] B. Hafez, A. S. Abdel-Khalik, A. M. Massoud, S. Ahmed, and R. D. Lorenz, "Single-sensor-based three-phase permanent-magnet synchronous motor drive system with Luenberger observers for motor line current reconstruction," *IEEE Trans. Ind. Appl.*, vol. 50, no. 4, pp. 2602–2613, Jul./Aug. 2014, doi: 10.1109/TIA.2013.2296625.
[34] M. A. M. Cheema, J. E. Fletcher, D. Xiao, and M. F. Rahman, "A direct thrust control scheme for linear permanent magnet synchronous motor based on online duty ratio control," *IEEE Trans. Power Electron.*, vol. 31, no. 6, pp. 4416–4428, Jun. 2016, doi: 10.1109/TPEL.2015.2475400.
[35] Y. Xu, H. Yan, J. Zou, B. Wang, and Y. Li, "Zero voltage vector sampling method for PMSM three-phase current reconstruction using single current sensor," *IEEE Trans. Power Electron.*, vol. 32, no. 5, pp. 3797–3807, May 2017.
[36] S. C. Yang, "Saliency-based position estimation of permanent-magnet synchronous machines using square-wave voltage injection with a single current sensor," *IEEE Trans. Ind. Appl.*, vol. 51, no. 2, pp. 1561–1571, Mar./Apr. 2015, doi: 10.1109/TIA.2014.2358796.
[37] S. Xiao, X. Gu, Z. Wang, T. Shi, and C. Xia, "A novel variable DC-link voltage control method for PMSM driven by a quasi-Z-source inverter," *IEEE Trans. Power Electron.*, vol. 35, no. 4, pp. 3878–3890, Apr. 2020, doi: 10.1109/TPEL.2019.2936267.
[38] X. Jin, J. Wang, Z. Yan, L. Xu, G. Yin, and N. Chen, "Robust vibration control for active suspension system of in-wheel-motor-driven electric vehicle via $\mu$-synthesis methodology," *J. Dyn. Syst., Meas., Control*, vol. 144, no. 5, May 2022, Art. no. 051007.
[39] K. D. von Ellenrieder, S. C. Licht, R. Belotti, and H. C. Henninger, "Shared human–robot path following control of an unmanned ground vehicle," *Mechatronics*, vol. 83, May 2022, Art. no. 102750, doi: 10.1016/j.mechatronics.2022.102750.

**QIANGGUO YU** was born in Hunan, China. He received the B.Sc. degree in electronic information engineering from Hunan University, Changsha, China, in 2000, and the M.Sc. degree in software engineering from Central South University, Changsha, in 2016.

Since 2020, he has been with Huzhou College, where he is currently a Senior Engineer. His current research interests include intelligent control and pattern recognition.

**YANAN FENG** was born in Anhui, China. He received the B.Sc. degree in electrical engineering from the Anhui University of Technology, Maanshan, China, in 2016, and the M.Sc. degree in electrical engineering from Southeast University, Nanjing, China, in 2019.

Since 2020, he has been with Huzhou College, Huzhou, China. His current research interest includes control of permanent magnet linear motor.

**XU HUANG** was born in Linyi, China, in 1977. He received the Ph.D. degree in computer science and technology from Soochow University, Suzhou, China, in 2011.

Since 2011, he has been with Huzhou University and Huzhou College successively. He is currently an Associate Professor with the major of computer science and technology. He is the author or coauthor of more than 40 technical articles. He is the holder of three patents in his areas of interest. His teaching and research interests include bioinformatics computing, parallel distributed computing, and swarm intelligence optimization algorithm.

**PEILIANG WANG** received the B.Sc. degree in industrial electrical automation and the M.S. degree in control theory and control engineering from Zhejiang University, Hangzhou, China, in 1986 and 2005, respectively.

From 2008 to 2009, he was a Visiting Scholar with Zhejiang University and the University of Duisburg–Essen, Germany, 2015. He is currently a Professor with the School of Engineering, Huzhou University, China, and a part-time Master's Tutor with Hangzhou Dianzi University and the Zhejiang University of Technology, China. His research interests include pattern recognition and intelligent control, process monitoring and diagnosis, and industrial automation. He is a member of the committee on the fault diagnosis and safety of technical process of the Chinese Association of Automation, the Executive Director and the Deputy Director of the Teaching Committee of the Zhejiang Association of Automation, and the Chairperson of the Huzhou Association of Automation.

**MENGJIA ZENG** was born in Jingzhou, China, in 1980. She received the master's degree in computer application technology from Xihua Normal University, Nanchong, China, in 2005.

Since 2014, she has been with Huzhou University, where she is currently an Assistant Professor with the School of Electronic Information. Her teaching and research interests include design, analysis, and control of electrical machines, using machine learning method to build model and optimization parameters.